Supporting Information

On the intrinsic dynamic nature of the rigid UiO-66 metal-organic framework

Julianna Hajek, Chiara Caratelli, Ruben Demuynck, Kristof De Wispelaere, Louis Vanduyfhuys, Michel Waroquier and Veronique Van Speybroeck

Center for Molecular Modeling (CMM), Ghent University, Technologiepark 903, B-9052 Zwijnaarde, Belgium

1. Methodology
1.1. General settings used in the MD simulations

In all simulations, the revPBE functional[1] with inclusion of Grimme D3 dispersion corrections[2] was chosen for its improved performance for solid-state calculations relative to the commonly used PBE functional.[3] PBE or revPBE – augmented with dispersion interactions - have shown to be successful in advanced or enhanced molecular dynamics (MD) calculations in periodic systems as they combine a relative accuracy with computing efficiency in the very demanding computer calculations.[4-9] The decision on the exchange-correlation functional has to be guided by a compromise between accuracy and computational cost, as correctly stated by Evans et al.[10] The usage of hybrid functionals such as B3LYP or PBE0 is fairly limited for systems with large unit cells as encountered here. To use such functionals for the enhanced sampling molecular dynamics methods performed here for a substantial number of configurations is beyond current computational limits. However, some interesting studies appeared to test the influence of the functional on the qualitative reliability of geometries and energies in recent literature, which give confidence that the same qualitative features as observed here would be found using other electronic levels of theory.[11-13] We used the DZVP-GTH basis sets for C, O and H atoms, which is a combination of Gaussian basis functions and plane waves (GPW) with a cut-off energy of 350 Ry. For Zr the DZVP-MOLOPT-SR basis set has been applied.[14] The simulations were performed in the NPT ensemble at 573 K and 1 bar. The time step for integration of the equation of motion was set to 0.5 fs. The temperature was controlled by a chain of five Nosé-Hoover thermostats,[15] the pressure by an MTK barostat.[16]

1.2. Determination of the collective variable in the dehydration process

The coordination number used in the simulation is formally defined as:

$$CN = \sum_{i=1,3} \frac{1 - \left(\dfrac{r_i}{r_0}\right)^6}{1 - \left(\dfrac{r_i}{r_0}\right)^{12}} \qquad (1)$$

where the index i labels each of the three Zr atoms surrounding the hydroxyl group as displayed in **Figure 2**. As reference distance r_0 for the Zr – O bond we take 2.7 Å.

The inspiration for the collective variable is based on the following arguments:

First of all, the reaction path towards dehydration has been studied earlier by static molecular simulation techniques, more specifically with Nudged Elastic Band (NEB) calculations.[17, 18] The intermediate states found in these static calculations give reliable suggestions on the structure of a suitable collective variable. More in particular some of the crucial intermediates found there are shown hereafter and clearly show the appearance of intermediate structures characters by partially decoordinated carboxylic groups, chelated ligands,… which are also observed here. However, from the static approach it is impossible to deduce the dynamic behavior of the linkers or to discriminate between a rotational or translational move of the ligands as was done here in the manuscript.
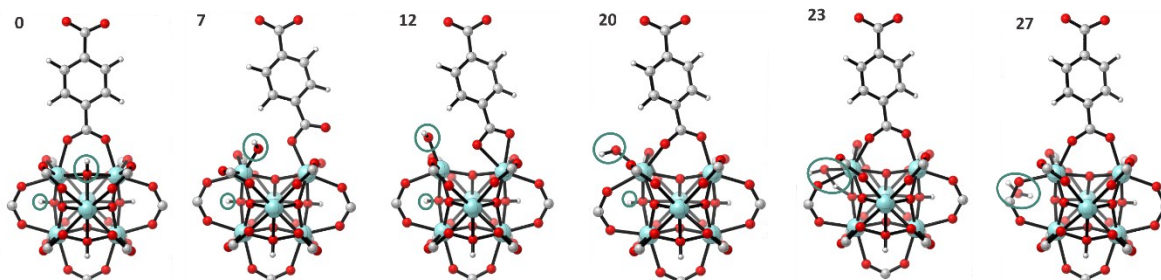
Secondly, we performed as part of the study published in reference 17 some regular MD simulations where we systematically increased the temperature to study the response of the material upon inserting energy in the system. At a temperature of 1273 K, we observed simultaneous decoordination of the μ_3-OH and one of the neighboring terephthalates. These observations were used to construct initial structures for the dehydration process studied with the NEB calculations. Of course, the temperatures necessary to induce the bond breakage there are unrealistically high, since the additional energy is distributed among all degrees of freedom of the system, yielding an overall swelling of the stable Zr-brick represented by $Zr_6O_4(OH)_4$ and eventually bond breakage between metal and bridging oxygen.

Apart from these observations, we also performed some preliminary metadynamics simulations with various collective variables, such as one or two distances between the oxygen of a bridging μ_3-OH group and the metal (see Figure 2). Such collective variables are less general and as such we only sampled part of the phase space visited during the US sampling method and some intermediate structures observed

here were also detected. As the system is highly dynamic, some elusive states of the system quickly rearranged into more stable configurations where for example water was formed. As such the required diffusive behavior for a sufficient sampling of the phase space was not reached. The US sampling method used here with the proposed collective variable, which does not impose any preference for one of the Zr atoms, allowed to obtain a sufficient sampling in the activated regions and to detect all possible motions of the ligands including rotation, translational modes. We checked that a sufficient overlap exists between the various umbrellas as described further in the Supporting information.

As the dehydration is an activated process regular AIMD simulations will need very long simulations times to observe this rare event. Therefore, this process can be enhanced by means of MD techniques with introduction of bias potentials pushing the system over the barrier. We have chosen umbrella sampling (US) as a suitable advanced MD technique to study this dehydration process. The procedure implies the partition of the whole reaction path into windows. In each window, an external harmonic bias potential is added to the true Hamiltonian to enhance the sampling in low probability regions. This done by performing MD simulations starting from initial structures specific for each window defined by the reaction coordinate.

A first exploration of the reaction path characterized by the collective variable (CV) (Eq.(1)) has been performed by means of a constrained MD simulation. In this simulation, a bias potential moves with a constant velocity along the reaction coordinate over the entire range of CVs (0.9 – 2.4). This constrained MD concept has been introduced by Grubmuller et al. [19] but it has not yet been applied in this context. After an equilibration run of 1 ps (2000 steps of 0.5 fs) the initial structure for the first window at CV = 2.4 is settled. The moving bias potential subsequently drives the system to lower values of the CV and this during 3 ps (6000 MD steps) simulation. The structure of the metal-organic framework adapts systematically at the new value of the CV. 36 snapshots are selected from this constrained MD simulations, more or less equally distributed over the remaining 6000 steps and thus the entire range of the CV (Table S1). Those snapshots will serve as input structures for the actual umbrella sampling simulations. The bias potential has a spring constant of κ = 1500 kJ·mol^{-1}·unit CV^{-2}.

To recombine the information of the various independent simulations, the weighted histogram analysis method (WHAM) [20] has been used.

1.3. The umbrella sampling simulations

In total 36 windows, corresponding to the 36 snapshots, have been introduced along the whole range of the CV. In each window, an umbrella sampling simulation has been performed for 25 ps with a starting configuration as extracted in the previous moving umbrella sampling procedure. The quality of the selection of the 36 windows along the reaction path and the magnitude of the spring constant characterizing the bias potential are assessed by sufficient overlap of the umbrellas covering the various windows. The results of our multiple umbrella samplings are clearly displayed in Figure S1. We observe that the range of the reaction path represented by 1.7 ≤ CV ≤ 2.4 is well covered, which is an indication that the sum of the three coordination numbers as CV is a well-suited choice in the reaction path towards the first transition state in the dehydroxylation. The region around CV = 1.6 seems less covered, indicating

the presence of some transition state. The post-transition region, which in our sampling is characterized by a CV smaller than 1.6, displays a somewhat less dense umbrella overlap. It should be noticed that the lower the value of the CV, the more fundamentally different configurations may generate the same value of the CV. This is inherent to the composition of the CV according to Eq. (1) which only takes into account the degree of coordination of the hydroxyl group. The number of sets $[r_1, r_2, r_3]$ yielding the same CV substantially increases at CV < 1.6 with large variations in the distances. The initial structure employed in each window is decisive for the type of configurations visited during the US in the phase space orthogonal to the collective variable.

Table S1: Specification of each umbrella with indication of the value of the collective variable (CV), step number in the constrained MD simulation. Spring constant κ = 1500 kJ·mol^{-1}·unit CV^{-2}.

Umbrella	CV	Step number	
u1	2.412992	2300	
u2	2.350807	2400	
u3	2.30496	2600	
u4	2.276639	3300	
u5	2.217113	3400	
u6	2.16906	3500	Configuration 1
u9	2.149121	4000	
u7	2.115	3600	
u11	2.000408	4400	
u10	1.962854	4200	Configuration 2
u12	1.913913	4950	
u13	1.853662	5000	
u14	1.807944	5100	
u16	1.779562	5300	
u15	1.74488	5200	
u17	1.723907	5700	
u8	1.641706	5850	Configuration 3
u18	1.596114	5800	
u19	1.519592	6050	
u20	1.508012	6150	Configuration of type 4, which leads to configuration 4r
u21	1.446838	6200	Configuration of type 4, which leads to configuration 4t
u22	1.410619	6300	
u23	1.371507	6650	
u24	1.35217	6700	
u27	1.332639	6900	
u26	1.301383	6800	
u29	1.288676	6950	
u25	1.278929	6750	
u30	1.261292	7050	
u28	1.228579	7000	
u31	1.161971	7100	

u32	1.10909	7200	
u33	1.044892	7400	
u34	0.994583	7500	
u36	0.951581	7700	
u35	0.939973	7600	Configuration 5

1.4. Reconstruction of the free energy surface

The free energy profile is constructed by application of the WHAM methodology.[21-23]

The value of the harmonic spring constant κ is fixed at 1500 kJ/mol for each umbrella sampling simulation. As depicted in Figure S1, this ad hoc choice for the harmonic constant generally yields sufficient overlap to construct a precise free energy profile, with respect to the window size.

On Figure S1 we see clearly some uncovered region around CV = 1.64, and it has a direct and visible impact on the free energy surface with a small bump at this window, which is unphysical, but which is difficult to remove. Starting an umbrella sampling in the windows just before and after this turning point the system systematically runs to a configuration further away from CV = 1.64. This feature is probably the result of the symmetric character of the chosen collective variable (Eq. (1)). An umbrella sampling on the reaction path does no further respect the symmetry between the three Zr atoms. The symmetry is broken once CV is lower than 1.64, i.e. moving from **configuration 2** to **configuration 3** (see main manuscript), and the system evolves in such an US simulation to a part of the free energy surface completely determined by the starting configuration of that umbrella.

Figure S1: Overview of the 5 ps umbrella sampling in the 36 windows which have been selected on the reaction path along the collective variable in the range 0.9 – 2.4. The bias potential has a spring constant of κ = 1500 kJ·mol^{-1}·unit CV^{-2}.
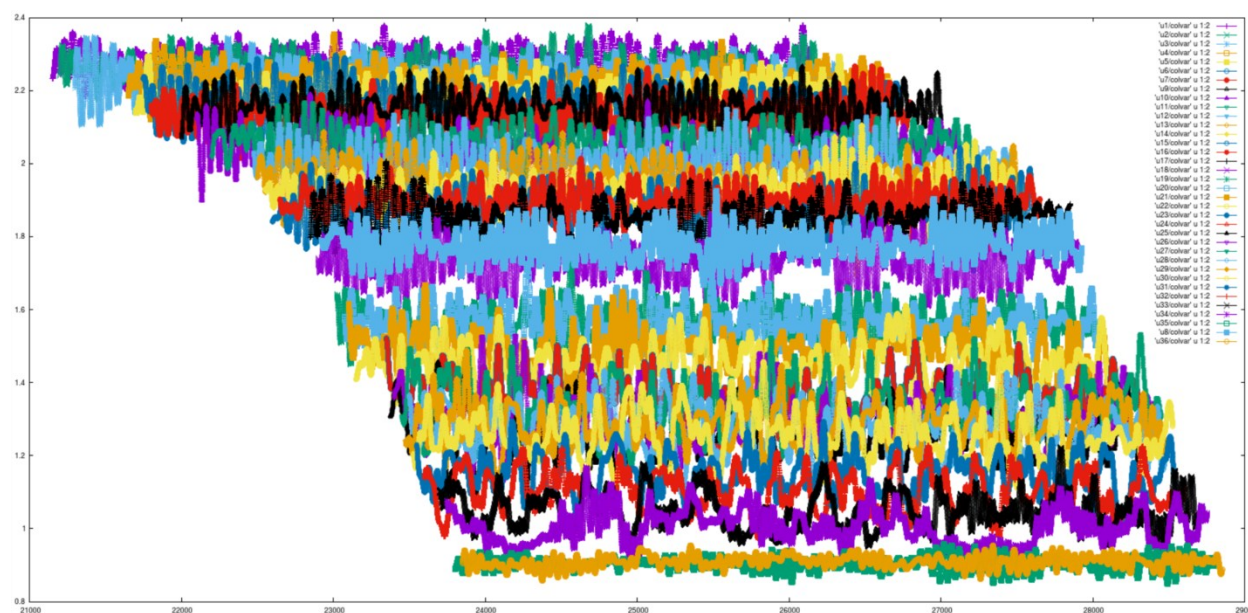
Table S2: Distances of Zr atoms to OH group

Distances of Zr atoms to OH group							
		Distance in the starting configurations [Å]			Average distances during the simulation [Å]		
Configuration	CV	Zr1	Zr2	Zr3	Zr1	Zr2	Zr3
1	2.17	2.32	2.26	2.31	2.30	2.30	2.30
2	1.96	2.14	2.51	2.56	2.38	2.39	2.38
3	1.64	2.58	2.32	2.97	2.51	2.56	2.54
4r	1.51	2.00	3.08	3.02	2.44	3.00	2.57
4t	1.45	2.17	2.98	3.10	2.27	3.55	2.59
5	0.94	2.07	4.80	4.13	1.97	2.97	4.84

2. Transition states observed during static NEB calculations

Figure S2: Transition states and free energy profile during dehydroxylation process taken from Vandichel et al. [17, 18]
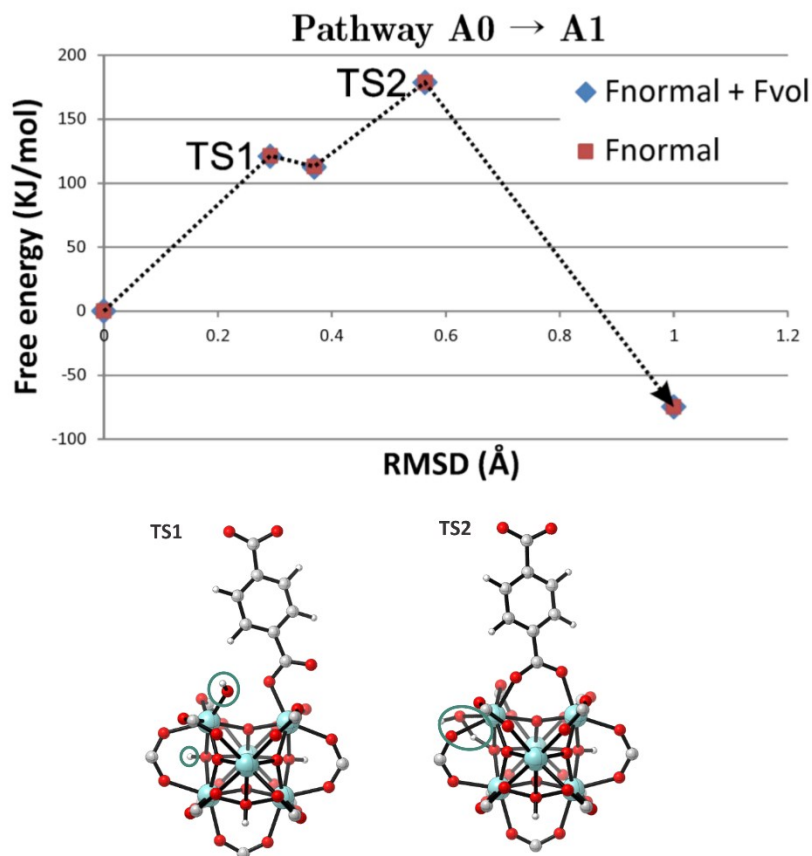
3. Intrinsic dynamic acidity of UiO-66

From Figure S3 we can see a rapid proton transfer involving the hydroxyl group and the carboxylic oxygen from the linker. When the interaction between the proton and the oxygen from the inorganic framework is strong the distance between the carboxylic oxygen and the proton is longer which results in a strong Zr-O binding interaction. When the proton is transferred to the carboxylic oxygen the distance between Zr-O is also weaker.

Figure S3: Changes of distance of proton disclosing the dynamic acidity in configuration 4r (for a better visibility we show 15 ps of the total 50 ps simulation time of regular MD).
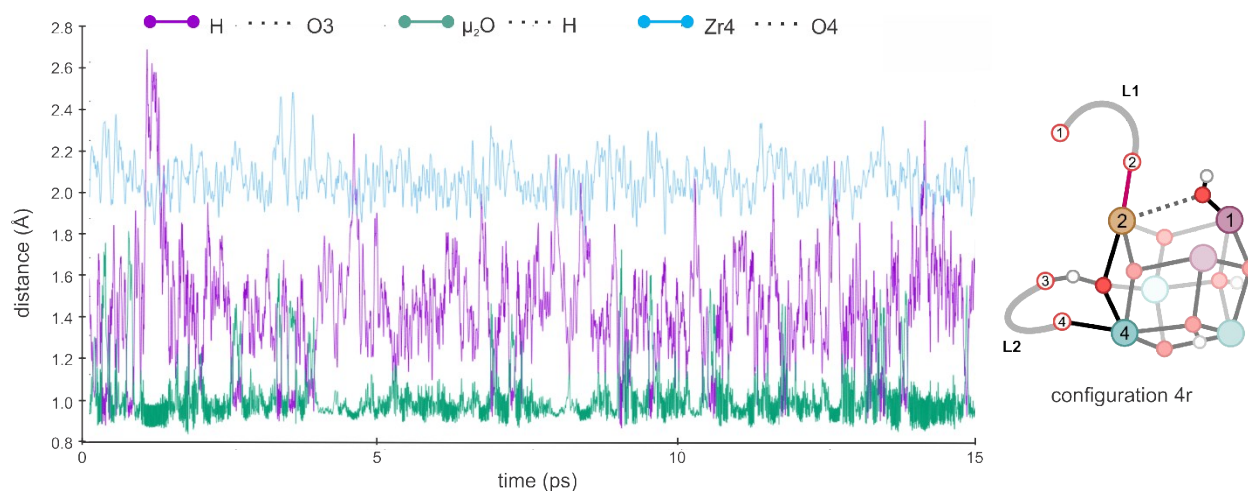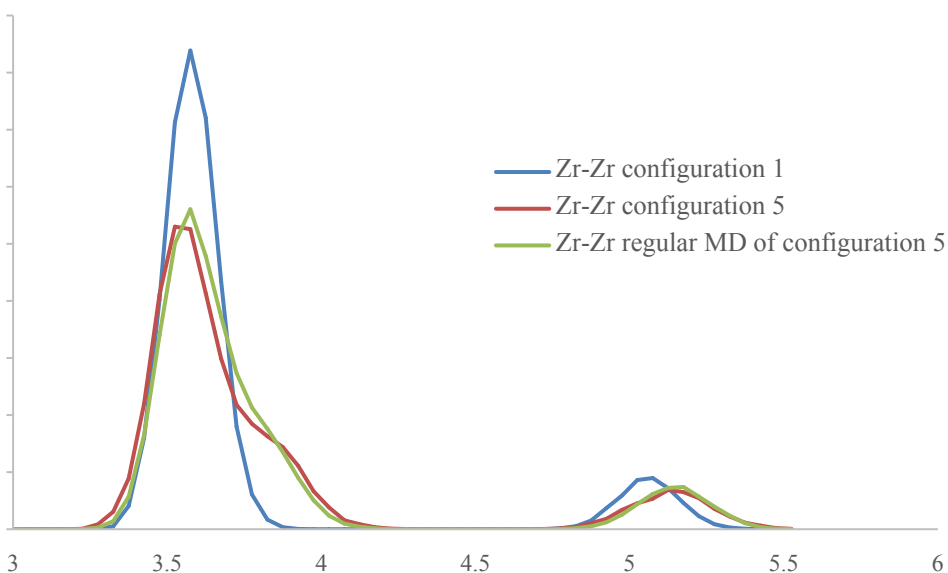

In Figure S3 the distance between the oxygen from the carboxylic group and the proton belonging to the μ_3-OH is indicated in purple. The distance which corresponds to the oxygen and the proton from the μ_3-OH is represented in green. We also display the bond distance of Zr and the oxygen atom from the carboxylic group (shown in blue).
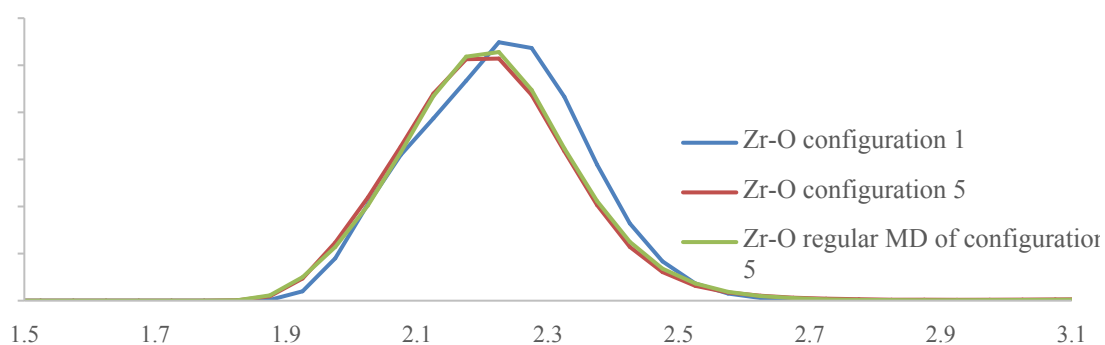
4. Distortions in the inorganic brick during activation process.

Figure S4: The distance between three Zr atoms from which the hydroxyl group is decoordinated is larger due to the lesser constraint of the hydroxyl group. The bond between oxygens and Zr atoms is almost preserved during the whole process.

Zr-Zr distances for the described brick

Legend: Zr-Zr configuration 1; Zr-Zr configuration 5; Zr-Zr regular MD of configuration 5

Zr-O distances for the described brick

Legend: Zr-O configuration 1; Zr-O configuration 5; Zr-O regular MD of configuration 5

1.   K. Yang, J. J. Zheng, Y. Zhao and D. G. Truhlar, *Journal of Chemical Physics.*, 2010, **132**, 10.
2.   S. Grimme, J. Antony, S. Ehrlich and H. Krieg, *Journal of Chemical Physics*, 2010, **132**.
3.   G. Lippert, J. Hutter and M. Parrinello, *Theoretical Chemistry Accounts*, 1999, **103**, 124-140.
4.   P. Cnudde, K. De Wispelaere, J. Van der Mynsbrugge, M. Waroquier and V. Van Speybroeck, *Journal of Catalysis*, 2017, **345**, 53-69.
5.   K. De Wispelaere, S. Bailleul and V. Van Speybroeck, *Catalysis Science & Technology*, 2016, **6,** 2686-2705.
6.   J. S. Martinez-Espin, K. De Wispelaere, M. W. Erichsen, S. Svelle, T. V. W. Janssens, V. Van Speybroeck, P. Beato and U. Olsbye, *Journal of Catalysis*, 2017, **349**, 136-148.
7.   J. S. Martinez-Espin, K. De Wispelaere, T. V. W. Janssens, S. Svelle, K. P. Lillerud, P. Beato, V. Van Speybroeck and U. Olsbye, *ASC Catalysis*, 2017, **7**, 5773-5780.

8.   C. Caratelli, J. Hajek, F. G. Cirujano, M. Waroquier, F. X. Llabrés i Xamena and V. Van Speybroeck, *Journal of Catalysis*, 2017, **352**, 401-414.
9.   C. Caratelli, J. Hajek, S. M. J. Rogge, S. Vandenbrande, E. J. Meijer, M. Waroquier and V. Van Speybroeck, *Chemphyschem*, 2017, DOI:10.1002/cphc.201701109.
10.   J. D. Evans, G. Fraux, R. Gaillac, D. Kohen, F. Trousselet, J.-M. Vanson and F.-X. Coudert, *Chemistry of Materials*, 2017, **29**, 199-212.
11.   V. Haigis, F.-X. Coudert, R. Vuilleumier, A. Boutin and A. H. Fuchs, *The Journal of Physical Chemistry Letters*, 2015, **6**, 4365-4370.
12.   S. Ling and B. Slater, *Chemical Science*, 2016, **7**, 4706-4712.
13.   J. Hajek, J. Van der Mynsbrugge, K. De Wispelaere, P. Cnudde, L. Vanduyfhuys, M. Waroquier and V. Van Speybroeck, *Journal of Catalysis*, 2016, **340**, 227-235.
14.   S. Goedecker, M. Teter and J. Hutter, *Physical Review B*, 1996, **54**, 1703-1710.
15.   D. Frenkel and B. Smit, *Understanding Molecular Simulation: From Algorithms to Applications*, 2001.
16.   G. J. Martyna, D. J. Tobias and M. L. Klein, *The Journal of Chemical Physics*, 1994, **101**, 4177-4189.
17.   M. Vandichel, J. Hajek, F. Vermoortele, M. Waroquier, D. E. De Vos and V. Van Speybroeck, *CrystEngComm*, 2015, **17**, 395-406.
18.   M. Vandichel, J. Hajek, A. Ghysels, A. De Vos, M. Waroquier and V. Van Speybroeck, *CrystEngComm*, 2016, **18**, 7056-7069.
19.   H. Grubmuller, B. Heymann and P. Tavan, *Science*, 1996, **271**, 997-999.
20.   S. Kumar, D. Bouzida, R. H. Swendsen, P. A. Kollman and J. M. Rosenberg, *Journal of Computational Chemistry*, 1992, **13**, 1011-1021.
21.   A. Grossfield, http://membrane.urmc.rochester.edu/content/wham.
22.   G. A. Tribello, M. Bonomi, D. Branduardi, C. Camilloni and G. Bussi, *Computer Physics Communications*, 2014, **185**, 604-613.
23.   S. Kumar, J. M. Rosenberg, D. Bouzida, R. H. Swendsen and P. A. Kollman, *Journal of Computational Chemistry*, 1992, **13**, 1011-1021.